HAL open science

Wildfire aerosol deposition likely amplified a summertime Arctic phytoplankton bloom

Mathieu Ardyna, Douglas S. Hamilton, Tristan Harmel, Léo Lacour, Diana N. Bernstein, Julien Laliberté, Christopher Horvat, Rémi Laxenaire, Matthew M. Mills, Gert van Dijken, et al.

To cite this version:

Mathieu Ardyna, Douglas S. Hamilton, Tristan Harmel, Léo Lacour, Diana N. Bernstein, et al.. Wildfire aerosol deposition likely amplified a summertime Arctic phytoplankton bloom. Communications Earth & Environment, 2022, 3, 10.1038/s43247-022-00511-9 . insu-03824434

HAL Id: insu-03824434

https://insu.hal.science/insu-03824434

Submitted on 21 Oct 2022

HAL is a multi-disciplinary open access archive for the deposit and dissemination of scientific research documents, whether they are published or not. The documents may come from teaching and research institutions in France or abroad, or from public or private research centers.

L'archive ouverte pluridisciplinaire **HAL**, est destinée au dépôt et à la diffusion de documents scientifiques de niveau recherche, publiés ou non, émanant des établissements d'enseignement et de recherche français ou étrangers, des laboratoires publics ou privés.

Distributed under a Creative Commons Attribution 4.0 International License

communications
earth & environment

ARTICLE

https://doi.org/10.1038/s43247-022-00511-9 OPEN

Wildfire aerosol deposition likely amplified a summertime Arctic phytoplankton bloom

Mathieu Ardyna [1,2,3,15]✉, Douglas S. Hamilton [4,5,15], Tristan Harmel [6], Léo Lacour [1,3], Diana N. Bernstein [7], Julien Laliberté[1], Christopher Horvat [8,9], Rémi Laxenaire [10,11,12], Matthew M. Mills [2], Gert van Dijken [2], Igor Polyakov[13,14], Hervé Claustre[3], Natalie Mahowald [4] & Kevin Robert Arrigo [2]

Summertime wildfire activity is increasing in boreal forest and tundra ecosystems in the Northern Hemisphere. However, the impact of long range transport and deposition of wildfire aerosols on biogeochemical cycles in the Arctic Ocean is unknown. Here, we use satellite-based ocean color data, atmospheric modeling and back trajectory analysis to investigate the transport and fate of aerosols emitted from Siberian wildfires in summer 2014 and their potential impact on phytoplankton dynamics in the Arctic Ocean. We detect large phytoplankton blooms near the North Pole (up to 82°N in the eastern Eurasian Basin). Our analysis indicates that these blooms were induced by the northward plume transport and deposition of nutrient-bearing wildfire aerosols. We estimate that these highly stratified surface waters received large amounts of wildfire-derived nitrogen, which alleviated nutrient stress in the phytoplankton community and triggered an unusually large bloom event. Our findings suggest that changes in wildfire activity may strongly influence summertime productivity in the Arctic Ocean.

[1] Takuvik Joint International Laboratory, Laval University (Canada) - CNRS (France), Département de biologie et Québec-Océan, Université Laval, Québec, QC G1V 0A6, Canada. [2] Department of Earth System Science, Stanford University, Stanford, CA 94305, USA. [3] Sorbonne Université & CNRS, Laboratoire d'Océanographie de Villefranche (LOV), 181 Chemin du Lazaret, F-06230 Villefranche-sur-Mer, France. [4] Department of Earth and Atmospheric Sciences, Cornell University, Ithaca, NY, USA. [5] Marine, Earth, and Atmospheric Sciences, North Carolina State University, Raleigh, NC 27695, USA. [6] GET (Université de Toulouse, CNRS, CNES, IRD, UPS), 14 avenue Edouard Belin, 31400 Toulouse, France. [7] Division of Marine Science, University of Southern Mississippi, 1020 Balch Blvd., Stennis Space Center, MS 39529, USA. [8] Institute at Brown for Environment and Society, Brown University, Providence, RI, USA. [9] Department of Physics, The University of Auckland, Auckland, New Zealand. [10] Laboratoire de Météorologie Dynamique, LMD-IPSL, UMR 8539 École Polytechnique, ENS, CNRS, Paris, France. [11] Laboratoire de l'Atmosphère et des Cyclones, LACy, UMR 8105, CNRS, Université de La Réunion, Météo-France, Saint-Denis de La Réunion, France. [12] Center for Ocean-Atmospheric Prediction Studies, Florida State University, Tallahassee, FL, USA. [13] International Arctic Research Center and College of Natural Science and Mathematics, University of Alaska Fairbanks, Fairbanks, AK, USA. [14] Finnish Meteorological Institute, Helsinki, Finland. [15] These authors contributed equally: Mathieu Ardyna, Douglas S. Hamilton. ✉email: Mathieu.Ardyna@takuvik.ulaval.ca

The intensity, frequency, and duration of fires is rapidly changing globally[1], altering the global carbon cycle and climate[1–3]. High latitude regions of the Northern Hemisphere (>50°N) have dense boreal forests and peatlands subject to major wildfire activity, emissions from which have approximately doubled (north of 60°) over the last decade[4]. The Arctic Oscillation-induced temperature increase appears to be critical for driving earlier snowmelt and fire activity, particularly in southeastern Siberia[5]. Aerosols and gases emitted from wildfires are predominantly carbonaceous in composition, but smoke plumes also carry significant amounts of bio-essential nutrients such as phosphorus[6,7], nitrogen (N)[8], and iron[9,10]. Although Russian observation stations do not routinely record information about N species, N deposition in other northern high latitude regions (e.g., North American High Arctic) is enhanced by wildfire smoke[11,12]. Consequently, wildfires can impact the Earth's biosphere by altering plant productivity, biodiversity, and ultimately ecosystem carbon storage[13,14].

Over the past two decades, wildfires have released substantial amounts of carbon in North America (60 Tg C $year^{-1}$) and Asia (124 Tg C $year^{-1}$)[15]. Major Arctic wildfire source regions include Canada, Scandinavia, and Russia[4], but also Greenland[16]. Russia accounts for approximately two-thirds of the total burnt area within these countries[4], highlighting the importance of understanding how changing fire activity in Russia under a warming climate could impact marine biogeochemical processes[17].

Depending on the type of vegetation burned, the return interval for boreal forest fires ranges from a few decades to many centuries[18]. Return intervals are projected to decrease in the future, leading to more frequent and severe fires. More severe fires have the potential to release more aerosol to the atmosphere per unit time burned, and thus nutrients deposited within their plumes can be expected to increase. The coupling of wildfires and marine biogeochemical cycles is a recent development in our understanding of the Earth System[19,20], and the impact of increasing boreal wildfires is yet to be assessed for Arctic Ocean marine primary production. Here, we suggest that boreal wildfires directly affect Arctic Ocean primary production by providing a new source of N, the macronutrient primarily limiting biological productivity in these waters[21,22], and thus stimulating phytoplankton growth[23].

Results

In summer 2014, ocean color satellites captured one prolonged, or several short, phytoplankton blooms (reaching 1–2 mg chlorophyll *a* m^{-3}, Fig. 1) up to 850 km south of the North Pole in the eastern Eurasian Basin. The pervasive cloud cover did not allow for continuous characterization of bloom dynamics, but snapshots of the ocean surface clearly revealed anomalously high chlorophyll *a* concentrations in the eastern Eurasian Basin, north of the Laptev Sea interior shelf. Given the spatial extent and short periods between missing retrievals, it was likely one single prolonged summer bloom. Also captured by satellite remote sensing were the exceptional sea ice conditions; although the onset of melt was two weeks later than the climatological mean, the consolidated ice pack disappeared in July and August at the most rapid rate ever recorded for this region and much further north (Fig. S1).

To ascertain the potential source of new nutrients fueling this high latitude bloom we assessed several plausible mechanisms (see the supplementary results for a comprehensive evaluation of all potential mechanisms) of new N supply to the N-depleted surface ocean in summer (Fig. S2). Summarizing, storm events can mix N-rich deeper waters to the surface; however, winds remained weaker than the 10 m s^{-1} threshold generally required to induce rigorous vertical mixing[24,25] (Fig. S3). Likewise, upwelling in the Arctic can transport deep nutrient-rich waters to the surface that support intense marine production[26–28]. The relative importance of this mechanism depends on regional factors such as sea ice cover, shelf depth, and wind direction with respect to the shelf break[29]. While upwelling favorable southeast winds over the Laptev Sea slope were observed in July–August 2014 (Fig. S3) they were moderate (max ~9 m s^{-1}). Furthermore, the strong topographically-controlled eastward boundary current (positive zonal component, Fig. S4) clearly inhibited shelf break upwelling in this region, as confirmed by temperature and salinity mooring data (Fig. S4). On the contrary, the temperature and salinity sections show a downwelling event along the shelf slope. Thus, we argue that neither storm-induced mixing nor shelf break upwelling provides the N that stimulated the observed bloom north of the Laptev Sea in summer 2014.

Ocean dynamics may trigger changes to phytoplankton growth rates. Polyakov et al. (2017)[30] argued that in recent decades (including 2014) increased vertical mixing in winter months (peaking in April) was driven by weakened halocline stratification and enhanced sea-ice production in the eastern Eurasian Basin. However, surface winter nutrient inventories are typically exhausted within two weeks by the spring bloom at the time of sea-ice retreat (which in 2014 began in early July; Fig. S1). Thus, any vertically mixed winter nutrients were likely exhausted prior to the onset of this late summer bloom. Further analyzing available records, we found a massive sub-surface anticyclonic eddy capable of introducing nutrients from deeper depths into surface waters (see section 2.3 in the Supplementary Notes; Figs. S5 and S6). However, its period of activity, low intensity in the upper water column, and position downstream of the current that influenced the bloom, suggest it had no effect on the bloom. The lateral advection of nutrients, particularly from river inflows, can be an additional source of new N to the open ocean. However, in situ studies clearly show that the Laptev Sea slope serves as a strong barrier preventing continental shelf waters from escaping into the deeper basin (especially in summer 2014 in the Laptev Sea[26–28]).

Excluding these physical mechanisms of N supply that increase phytoplankton growth promotes the hypothesis that an increased nutrient supply from the atmosphere supported the observed phytoplankton bloom. During the summer intense wildfires extend over large areas of boreal forests and peatland (Fig. S7), producing extensive smoke plumes that include N compounds (i.e., nitrous oxide, nitrite, and ammonia). Analysis shows Arctic wildfire activity and pollution enhancements are most pronounced in July and August[31,32], when the 2014 bloom was observed. The region 115–125°E and 60–70°N, within the Sakha (Yakutia) Republic in Russia, is directly upwind of the observed bloom and MODIS recorded a burnt area (1486 kha) in July and August (Fig. 4a) that was approximately three-fold higher than the decadal average (Fig. S8). Furthermore, this examined Sakha Republic region is 7.5× smaller than Canada above 60°N, but the area burnt there in 2014 was two-thirds of the total area burnt in Canada above 60°N (Fig. S8 and Supplemental Text). The 2014 fires in Sakha, Russia were exceptionally large, and thus may provide an indication of future fire behavior.

Atmospheric circulation can transport continental wildfire smoke from Russia northwards to the Arctic Ocean. The Copernicus Atmosphere Monitoring Service (CAMS) reanalysis dataset (Fig. 2) and satellite images combined with back-trajectory analysis (Fig. 3b) both show how wildfire smoke emitted from Russia (Fig. 3a) traveled over the Laptev Sea and the eastern Eurasian Basin to reach the anomalous Arctic bloom of August 2014. Tiksi (128.9°E, 71.6°N; 1 m above sea level) is a remote coastal Siberian measurement station situated along this transport path. During the summer of 2014, four clear aerosol

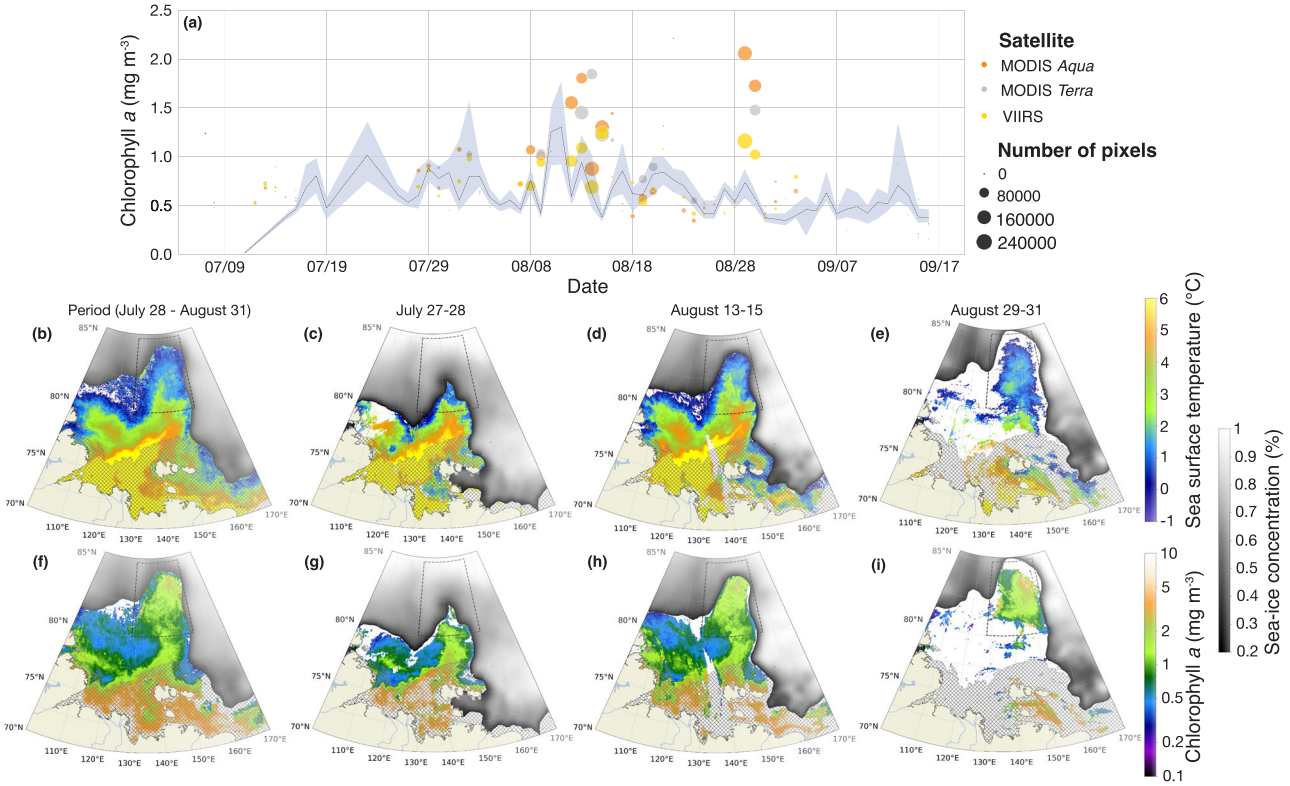

Fig. 1 Large summer phytoplankton bloom near the North Pole (eastern Eurasian Basin) in summer 2014. Satellite-derived mean chlorophyll *a* concentration within the region of the bloom (28–155°E, 80–85°N) during the summer of 2014 (**a**). Dot color represents which satellite sensor (MODIS Aqua, Terra, or VIIRS) is used. Dot size is relative to the number of observations obtained (i.e., pixels). The blue line is the climatological daily average of surface chlorophyll *a* concentration over the period 2003–2019 (except 2014) with the shading envelope corresponding to the interval between the first and third quartiles. Sea-ice concentration and sea surface temperature, for the full period July 28–August 31 (**b**), and for the three time periods July 27–28, August 13 –15, and August 29–31 (**c**–**e**, respectively). Sea-ice concentration and chlorophyll *a* concentration, for the same dates as **b**–**e**, shown in panels **f**–**i**. For **b**–**i**: location of the bloom is within the dotted box (28–155°E, 80–85°N) and the continental shelf (bottom depth <50 m) is shown by cross-hatching.

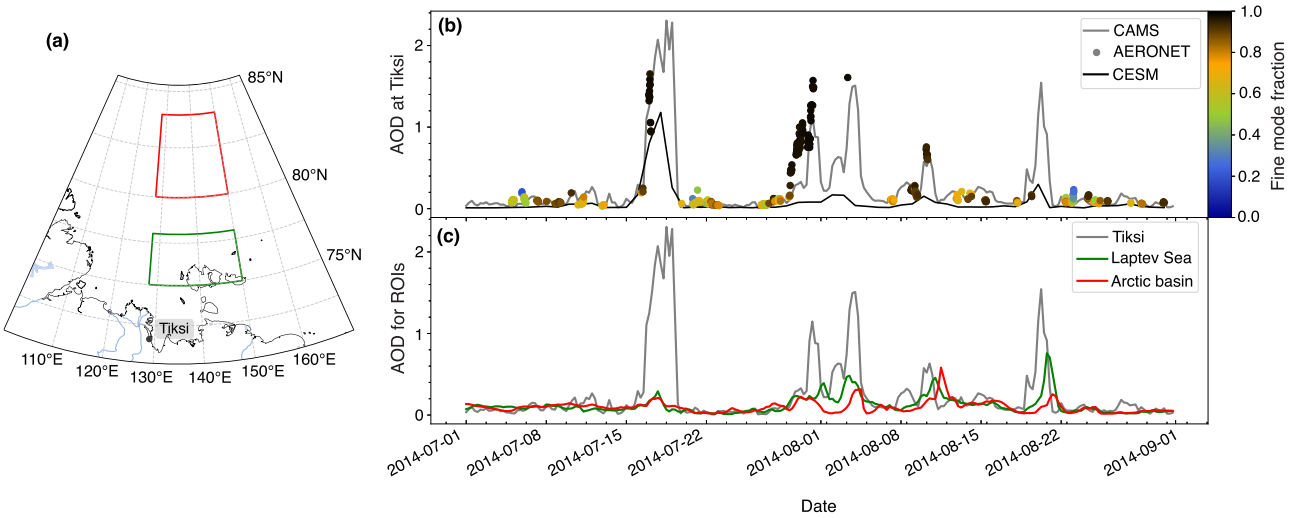

Fig. 2 Aerosol content over ground reference site and region of interest. Locations of the different regions of interest (**a**). Comparison of the aerosol optical depth at 550 nm based on AERONET measurements (level 2.0), CAMS archive, and CESM simulations with FINN fire emissions over the Tiksi-AERONET site (**b**). The color scale indicates the fraction of fine mode aerosol contributing to AOD as retrieved from the AERONET-Solar processing. Spatially averaged AOD for the regions of interest (**c**).

peaks (aerosol optical density; AOD) were recorded at Tiksi. All AOD peaks are dominated by fine mode aerosols indicative of a wildfire source, as opposed to coarse mode aerosol which would indicate other local natural aerosol sources (e.g., sea spray or dust). High elemental carbon (EC) concentrations measured at Tiksi (Fig. S9) further support the domination of AOD by fire aerosols. CAMS AOD over the bloom, and over the Laptev Sea en route to the bloom, shows three August peaks (Fig. 2). A time-lag between the original Tiksi AOD peak and two subsequent AOD peaks en route suggests that the smoke was transported

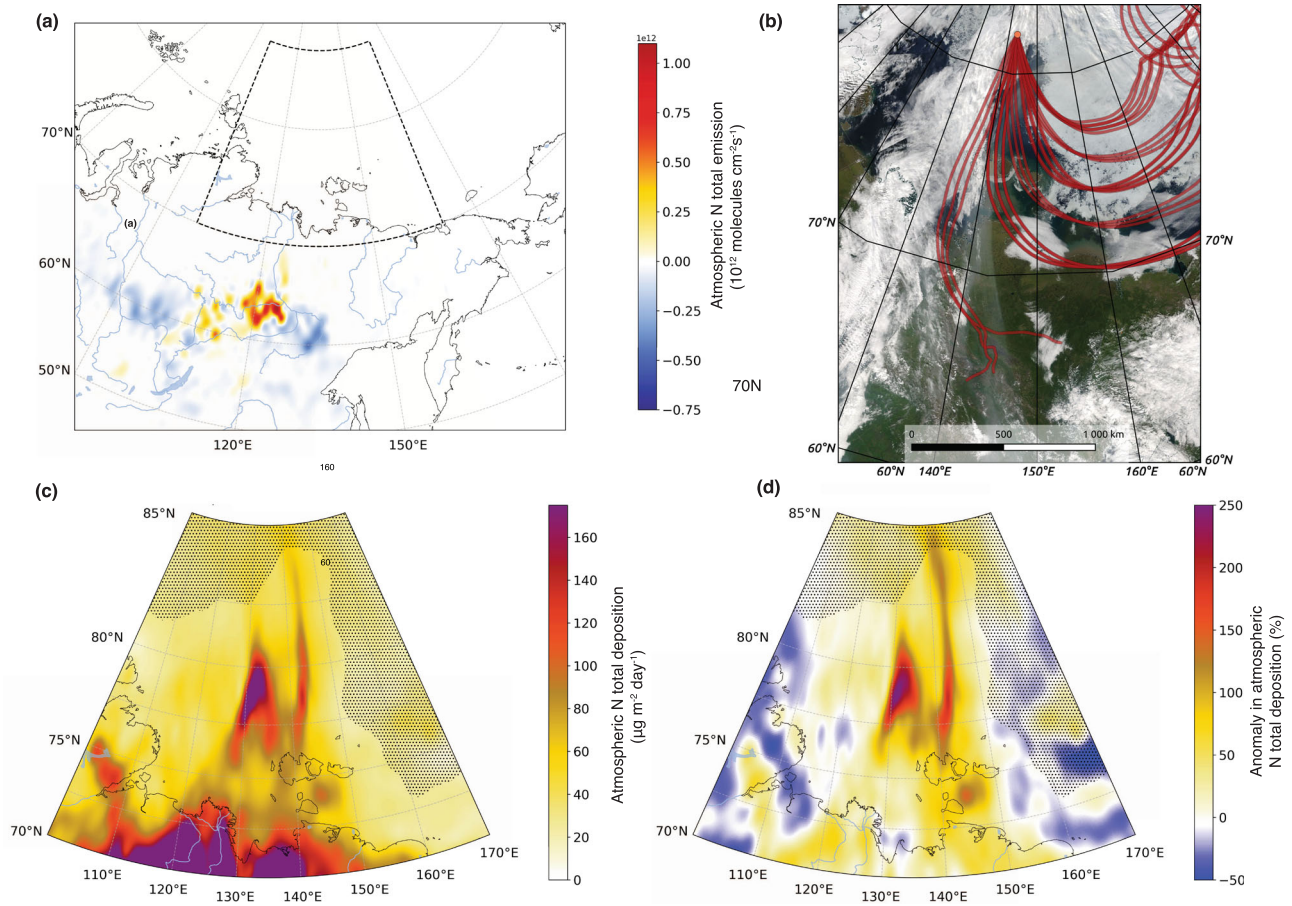

Fig. 3 Wildfires in Siberia, from nitrogen emissions to deposition in the eastern Eurasian Basin. Modeled FINN fire emissions of N (July 15–August 14 2014 anomaly versus the 2002–2019 mean) (**a**) with a box showing the location of panels (**c**, **d**). MODIS visualization of the aerosol plume and corresponding HYSPLIT back-trajectories highlighting atmospheric transport pathways (in red) to the location of the bloom (**b**). Simulated N deposition flux in 2014 (**c**) and the related deposition anomaly versus the 2011–2016 mean N deposition flux (**d**).

from the continent to the bloom over a couple of days (see also: Fig. S10). However, the mid-July AOD peak at Tiksi is not observed over either Arctic Ocean region of interest, suggesting that smoke from fires in early July may have taken a different trajectory than later in July and August.

The Community Earth System Model (CESM; see "Methods")[33] includes N deposition from wildfires and is used here to estimate N deposition fluxes to the Artic Ocean. Simulations suggest that in late July–August 2014, N deposition fluxes were anomalously high (Fig. 3c), reaching over double that of the preceding and following years (Fig. 3d). Fires and plume transport directions are episodic[34] (Fig. S10), and results show five consecutive deposition pulses, including one strong pulse in late July, three smaller pulses in early August, and one final large pulse on 21 August (Fig. 4b). Since Arctic Ocean waters are relatively stratified compared to other ocean basins, the estimated residence time of these atmospherically deposited aerosols could be sufficiently long to allow any associated N to accumulate, over a period of days[35], to a sufficiently high enough concentration for phytoplankton uptake and subsequent growth.

To assess whether the fires provided sufficient exogenous N to enhance production, we established a nutrient budget for the region based on current models of atmospheric N deposition (Table 1). Several lines of evidence suggest that the Fire INventory from NCAR (FINN) emission dataset[36], used here in CESM simulations, likely underestimates boreal fire emissions. First, McCarty et al. (2021)[4] showed that Arctic FINN fire emissions are between a factor of 2–5 lower than all other major fire emission inventories. Next, while the CAMS reanalysis dataset reproduces AOD observations at Tiksi (Fig. 2), both in magnitude and timing, atmospheric modeling of aerosol transport using FINN emissions in CESM captures only the timing of the AOD peaks; the AOD magnitude is lower than both CAMS and observations by a factor of 2–5, with the best-captured peak being the first one which may not have reached the bloom. In addition, Eckhardt et al. (2015)[37] showed that global modeling, on average, underpredicts measured aerosol observations of EC taken at Tiksi by a factor of 3. Finally, CESM CO concentrations (a tracer of combustion) are lower than pan-Arctic observations by the same factor of ~2–5 (Fig. S11). Applying adjustments of 2–5× suggests that wildfires provided between ~12 and 30% (Table 1: standard model ×2 and ×5) of the N required to fuel the enhanced biomass associated with the bloom. However, the atmospheric deposition model we used is missing a significant source of N in sub-polar environments from N-rich peat fires (Fig. 4a), which are not represented in the FINN emission dataset. Assuming a ×3.5 factor is required to account for additional N emissions from peat fires (see "Methods"), the successive N deposition events we observed in the summer of 2014 could then support between ~40 and 100% of the total N content of the bloom (Fig. 4b and Table 1). Despite uncertainties in our knowledge of N emissions, and subsequent atmospheric deposition to aquatic ecosystems, the budget reconciles N transport when including peat fires in this region. Thus, in very N-depleted and highly stratified conditions in the Arctic Ocean, especially in the Central Arctic, significant deposition of N from peat fires will likely impact Arctic Ocean phytoplankton growth and productivity.

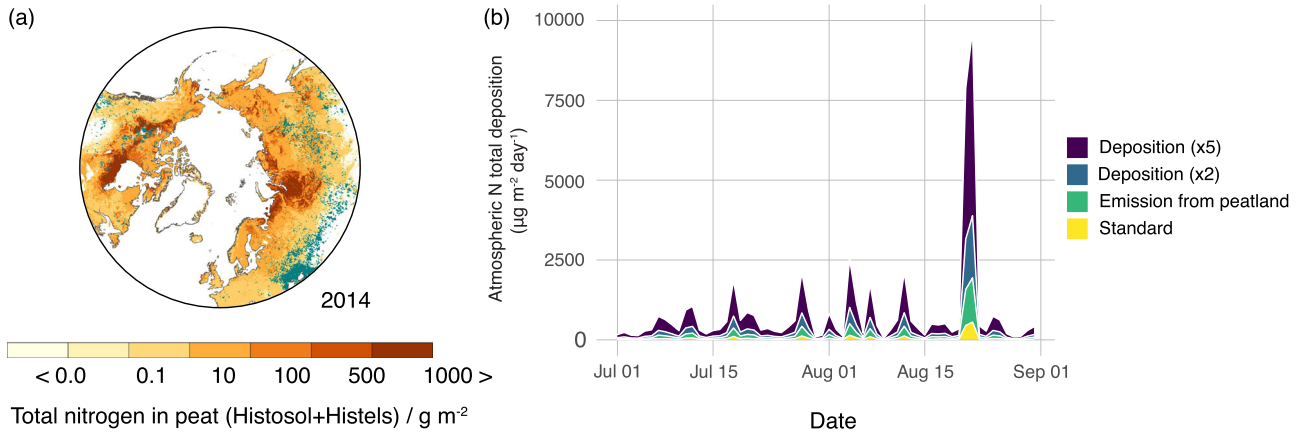

Fig. 4 Nitrogen stock in boreal peat reserves and deposition in the region of the bloom (longitude: 128–155°E; latitude: 75–85°N). Stocks and spatial distribution of nitrogen contained in boreal peat reserves (**a**) and 2014 wildfire locations (a; teal dots). Time series of the estimated magnitude of nitrogen wet and dry deposition integrated over the region (128–155°E, 75–85°N) from CESM simulations (**b**). Uncertainty in deposition fluxes is estimated from missing peat burning emissions and the fire inventory uncertainties (factor of 2–5). Values given in Table 1 are the integrated deposition fluxes as shown here. Nitrogen in peat from Hugelius et al. (2020)[46]. Wildfire locations from MODIS where burnt area was > 0 in July and August 2014.

Table 1 Nitrogen budget for wildfire aerosol fueled Eastern Eurasian Basin phytoplankton bloom.

Eastern Eurasian Basin phytoplankton bloom 2014	
Accumulated chlorophyll *a* (mg m^{-3})	0.7 ± 0.3[a]
MLD (m)	10.0 ± 5[b]
Integrated chlorophyll *a* (mg m^{-2})	7.0 ± 4.6
Chlorophyll *a*: N (mg: mmol N)	2.0 ± 2[c]
N requirement (mmol N m^{-2})	**3.5 ± 6.4**
Total N deposition July 1–Aug 31, 2014 (mmol N m^{-2})	
Standard Model	0.2 ± 0.4
Inclusion of peat biomass	0.7 ± 1.4[d]
Base deposition estimate (Inclusion of peat fires ×2)	1.4 ± 2.8[e]
High deposition estimate (Inclusion of peat fires ×5)	3.5 ± 70.0[e]
N requirement met by wildfire aerosol deposition (%)	
Standard Model	5.7 ± 15.5
Inclusion of peat biomass	20.0 ± 54.3
Base deposition estimate (Inclusion of peat fires ×2)	39.9 ± 108.6
High deposition estimate (Inclusion of peat fires ×5)	99.8 ± 271.5

Note: [a]determined as difference between the average chlorophyll *a* concentration during the period of peak bloom (indicated in Fig. 1a shaded region) and the pre-bloom period before 7/16/2014, [b]defined based on NABOS expeditions in the Laptev Sea (see Fig. S2), [c]estimated using in situ data collected during ICESCAPE 2010[69] and 2011[69] as well as results from ref. [70] and ref. [71], [d]inclusion of the specificities of peat biomass, i.e., N and $PM_{2.5}$ concentrations are up to ~3.5 times higher than emissions from boreal[8] and tropical[67] forest fires, [e]2 to 5-fold uncertainty exists in modeled deposition estimates[31] (e.g., Figs. 2 and S7).

Discussion and conclusions

Here, our objective is not to demonstrate that this unusual summer bloom is entirely explained, or triggered, by the wildfire aerosol N deposition, but rather that it is most likely a significant contributor to its development and/or duration. Other mechanisms have been investigated and excluded as potential significant N sources, but it is plausible that other unidentified N sources may contribute to this unusually long bloom in the highly stratified and oligotrophic eastern Eurasian Basin. Nevertheless, the potential importance of wildfire aerosol deposition as an emerging mechanism in modulating Arctic Ocean biogeochemical cycles needs to be highlighted. Under the effect of climate change, these deposition events can supply surface waters with significant levels of nutrients, as in other ocean basins[38,39]. It is very likely that future fire-related deposition events will become more frequent and intense, with increasingly severe wildfires in peatlands and boreal forests. However, episodes of high fire activity remain unpredictable and are thus difficult to measure; from the deposition of aerosols to their impact on biogeochemical cycles, which may have a time-lag of several days[35]. The impact of wildfires (and more specifically aerosol deposition) on sea ice thermodynamic and dynamic properties is not investigated here, although they are likely to be interconnected[40,41]. Soot and associated nutrients from wildfires deposited on ice can (1) lead to increased melting by reducing its albedo, (2) be transported over large distances with sea ice (even in the Central Arctic) and, (3) when the ice melts, increase nutrient and freshwater fluxes that stratify the water column and make the upper ocean more suitable for phytoplankton growth. Given the degree to which shifts in sea ice surface properties can drive large-scale changes in under-ice ecology[42,43], understanding the effects of wildfire-driven changes to sea ice, and the related effect on Arctic ecosystems, ought to be explored in future work.

Knowledge about atmospheric aerosol nutrient sources and deposition patterns is scarce at the pan-Arctic scale, with nearly all marine aerosol nutrient observations being collected below the Arctic circle[44,45]. Significant reserves of all peatland N (~80%) are currently stored within northern high latitude peatlands[46] (Fig. 3a). Global warming is projected to result in reductions to the permafrost of peatlands by 50–100% with a warming of 2–6 °C relative to preindustrial times[46]. If increases in precipitation do not offset soil moisture losses through warming, then vegetation water stress increases and peatlands dry further and faster, making fuel more combustible and leading to an overall elevated risk in sustained major fire outbreaks. In this study, global climate model simulations, including N species contained in wildfire smoke, are used to test the hypothesis that Arctic biogeochemical cycles are sensitive to changes in boreal wildfire activity. However, the 2014 wildfires only occurred within regions of moderate peatland N stocks (Fig. 4a). Wildfires have been detected within regions containing peatland with a higher N store (Fig. S7), and thus future increased boreal wildfire activity combined with a more readily mobilized N stock from thawed peatland may rapidly amplify impacts of human perturbations to Arctic ecosystems. Russian burnt area accounts for ~2/3 of all high latitude regions combined in the present day[4], yet it is understudied when compared to North America. Different N

species have different atmospheric lifetimes and thus transport potential. The N species contained in smoke plumes is thus likely to be an additional important consideration in determining the changing contribution of wildfires to aerosol burdens and marine fluxes in different Arctic regions[47]. Increased observational efforts will thus improve model simulations and provide a better understanding of the impact of boreal wildfires on Arctic Ocean productivity.

Considering the N-depleted nature of Arctic Ocean surface waters, N-bearing aerosol deposits originating from wildfires will undoubtedly have repercussions on the nutrient and carbon cycles. Especially during the summer, when phytoplankton growth is severely N-limited[4], these new N inputs could stimulate phytoplankton productivity and may partly explain the ongoing increase in annual primary production in the Arctic Ocean[48,49]. Phytoplankton growth is controlled by many factors, both physical and biogeochemical. Aerosol deposition, including from wildfires, is a source of new nutrients in many remote ecosystems[50]. In this study, global aerosol transport modeling suggests that Siberian wildfires supplied between 12 and 100% of the required N to support a large Arctic bloom in the summer of 2014, with the mass of N emitted from peat fires identified as a main uncertainty. Yet, nutrient aerosol addition may not always result in increased primary productivity[17]. Addressing the question of what initial conditions support aerosol-mediated phytoplankton growth should be explored further and will aid in understanding the evolution of the biogeochemical couplings between the land, ocean, and atmosphere under human-mediated climate change. These amplifying climate-driven changes, in addition to late summer/fall storms, will certainly promote secondary/fall blooms and thus contribute to the potential borealization of Arctic marine ecosystems[25,51]. The cascading effects of wildfire aerosols on different components of the Arctic ecosystem (land, atmosphere, sea ice, and ocean) create multiple questions that need to be assessed, quantified, and integrated into Arctic studies, in order to understand their implications on marine biogeochemistry in a changing global climate.

Methods

Ocean color and surface parameters

Ocean color. Chlorophyll *a* concentration, was inferred from retrievals of the three main ocean color satellite missions in orbit over the time period of this study (2014): MODIS-Aqua, MODIS-Terra, and VIIRS-SNPP; note that similar processing was used to generate the daily chlorophyll *a* climatology using satellite data available between 2003 and 2019. The composite products of the three missions were generated based on the recommendations of the *Ocean Color - Climate Change Initiative*[52], but for a finer spatial resolution corresponding to a pixel edge of ~1 km. The remote sensing reflectance R_{rs} and chlorophyll *a* were obtained after atmospheric correction performed through the SeaDAS software[53] and the combination of the spectral ratio and color index algorithms for chlorophyll *a*[54,55]. Note that the latter parameter was also estimated through regionally-tuned algorithms showing similar results (see Fig. S12). Image reprojection, binning, and aggregation were performed using the *Sentinel Application Platform* (SNAP) software, developed by *Brockmann Consult*.

Thanks to the high number of data acquisitions in this period (up to 8 for a given satellite per day), bad quality pixels were filtered out, and basic statistics were performed to provide quality controlled daily values. First, for each individual image, pixels were filtered out if one of the following quality flags provided by the SeaDAS algorithm is true: ATMWARN, ATMFAIL, HIGLINT, HILT, HISATZEN, STRAYLIGHT, CLDICE, CHLFAIL, and MAXAERITER. Due to particularly complex environmental conditions in Arctic seas for optical remote sensing, another pixel filtering procedure was performed when at least one the spectral bands exhibited R_{rs} values smaller than 0.0003 sr^{-1} or if the ratio between R_{rs} at 412 and 443 nm was >2.5. Note that pixels with aerosol optical thickness >0.2 were also filtered out to avoid misinterpretation of pixel information in the presence of aerosol plumes from the wildfires. The second step consists of calculating the daily median and standard deviation values for each pixel location of a given satellite mission. Once the daily product is obtained, the composite image was constructed by averaging the pixel values of the three distinct satellite missions.

Sea surface temperature. The SST was obtained from the MODIS-Aqua level-2 NASA products derived from long-wave (11–12 μm) thermal radiation. Daily SST images were generated following the similar approach to that applied for the ocean color products but using the following flags to filter out bad quality pixels: BTDIF, SSTRANGE, BTNONUNIF, CLOUD.

Atmospheric transport modeling. CESM version 1.5[33] was used with the interactive chemistry version of the Community Atmospheric Model (CAM-chem) as the atmospheric component[56] following the set-up described in Bernstein et al. (2021)[57]. Aerosols in CAM-chem are represented by four modes (Aitken, accumulation, coarse, and a primary carbon)[58]. All simulations were performed on a horizontal resolution of 0.9 × 1.25° and 56 vertical levels with offline meteorology nudged to GEOS5[59] meteorological analysis. Dust and sea salt are prognostically calculated following the MAM4 default configuration[58]. Anthropogenic emissions are taken from HTAP-2[60]. Daily fire emissions (from wildfires, agricultural fires, and prescribed burning) are taken from the Fire INventory from NCAR (FINN) dataset[36] version 1.6 and prescribed vertically following AeroCom recommendations[61] up to a maximum plume height of 5 km.

The CAMS reanalysis dataset incorporates satellite-derived AOD reanalysis using the ECMWF Integrated Forecasting System[62]. In this way, CAMS reduces bias with observations, and in the context of this study, provides an AOD reference with which to compare CESM results. The Hybrid Single-Particle Lagrangian Integrated Trajectory model (HYSPLIT)[63], developed by NOAA's Air Resources Laboratory, was used to simulate back trajectories from the location of the bloom (82°N, 130°E, August 12, 2014).

Current fire emission inventories combine data from different sources, on fire fuel loading, biomass consumed, and species-specific emission factors to estimate emissions over the area burned. This results in substantial uncertainties between commonly used datasets which differ by a factor of 4 globally and by factors of 3–15 regionally[64,65]. A second uncertainty is that when fire emissions are prescribed in global model simulations, there is a well-known low bias compared to aerosol optical depth measurements[2,66], leading to regional adjustments of fire emissions commonly between a factor of 2–3.

The fire emission database FINN used here does not include peatland fire emissions, and thus model simulations do not transport any N from peat fires, despite fires occurring within regions containing peatlands (Fig. 4a). For our study region, FINN currently contains the lowest estimates of fire carbon emissions between all inventories: the highest estimates being a factor of ~5 larger[14]. In addition to peat fires being a large missing carbon source they are also a significant missing source of nitrogen owing to some species (e.g., HCN and NH_3) being emitted from smoldering peat fires at a factor of ~10 higher, per unit biomass consumed, than for flaming savanna fires[8] or a factor of 3.5 higher than boreal fires[8]. Therefore, to estimate the missing source contribution of peat fires to the N deposition flux, an emission ratio of 3.5 (peat fires:boreal fires) is used as a bias correction, based on emission factor differences between boreal forests and peatlands for some N species[8] and the missing $PM_{2.5}$ contribution from tropical peatland fires when using the FINN dataset[67]. Assuming linearity in transport of peat fire emissions with those from forest fires, we applied this factor 3.5 bias correction factor to the 'inclusion of peat biomass' nitrogen deposition flux in Table 1. Burned area was estimated using the collection 6 MODIS Global Burned Area Product MCD64CMQ (climate model grid)[68].

Data availability

The NABOS oceanographic dataset in the Laptev Sea was obtained from https://uaf-iarc.org/nabos/. AERONET data for the Tiksi site (PI: Brent Holben) were downloaded from https://aeronet.gsfc.nasa.gov/. Ocean color data from MODIS-Aqua, MODIS-Terra, and VIIRS-SNPP and sea surface temperature from MODIS-Aqua were downloaded from https://oceancolor.gsfc.nasa.gov and https://ladsweb.modaps.eosdis.nasa.gov. The sea ice concentration and melt onset dates were obtained from the NSIDC (https://nsidc.org). The daily CESM aerosol optical depth and nitrogen deposition data for July and August 2014 used in this study can be downloaded from https://doi.org/10.5281/zenodo.6862522. We use the NASA collection 6 MODIS Global Burned Area Product MCD64CMQ to estimate burnt area in each year, which is available to download from https://modis-land.gsfc.nasa.gov/burn.html. Nitrogen content in peatlands was taken from Hugelius et al. (2020)[46].

Received: 28 May 2021; Accepted: 27 July 2022;
Published online: 19 September 2022

References

1. Li, F. et al. Historical (1700–2012) global multi-model estimates of the fire emissions from the Fire Modeling Intercomparison Project (FireMIP). *Atmos. Chem. Phys.* **19**, 12545–12567 (2019).
2. Ward, D. S. et al. The changing radiative forcing of fires: Global model estimates for past, present and future. *Atmos. Chem. Phys.* **12**, 10857–10886 (2012).
3. Andela, N. et al. A human-driven decline in global burned area. *Science* **356**, 1356–1362 (2017).

4. McCarty, J. L. et al. Reviews and syntheses: Arctic fire regimes and emissions in the 21st century. *Biogeosciences* **18**, 5053–5083 (2021).
5. Kim, J.-S., Kug, J.-S., Jeong, S.-J., Park, H. & Schaepman-Strub, G. Extensive fires in southeastern Siberian permafrost linked to preceding Arctic Oscillation. *Sci. Adv.* **6**, eaax3308 (2020).
6. Mahowald, N. et al. Global distribution of atmospheric phosphorus sources, concentrations and deposition rates, and anthropogenic impacts. *Global Biogeochem. Cy.* https://doi.org/10.1029/2008gb003240 (2008).
7. Barkley, A. E. et al. African biomass burning is a substantial source of phosphorus deposition to the Amazon, Tropical Atlantic Ocean, and Southern Ocean. *Proc. Natl. Acad. Sci. USA* **116**, 16216–16221 (2019).
8. Andreae, M. O. Emission of trace gases and aerosols from biomass burning—an updated assessment. *Atmos. Chem. Phys.* **19**, 8523–8546 (2019).
9. Guieu, C., Bonnet, S., Wagener, T. & Loÿe-Pilot, M.-D. Biomass burning as a source of dissolved iron to the open ocean? *Geophys. Res. Lett.* https://doi.org/10.1029/2005gl022962 (2005).
10. Hamilton, D. S. et al. Improved methodologies for Earth system modelling of atmospheric soluble iron and observation comparisons using the Mechanism of Intermediate complexity for Modelling Iron (MIMI v1.0). *Geosci. Model Dev.* **12**, 3835–3862 (2019).
11. Kharol, S. K. et al. Dry deposition of reactive nitrogen from satellite observations of ammonia and nitrogen dioxide over North America. *Geophys. Res. Lett.* **45**, 1157–1166 (2018).
12. Wentworth, G. R. et al. Ammonia in the summertime Arctic marine boundary layer: Sources, sinks, and implications. *Atmos. Chem. Phys.* **16**, 1937–1953 (2016).
13. Pellegrini, A. F. A. et al. Fire frequency drives decadal changes in soil carbon and nitrogen and ecosystem productivity. *Nature* **553**, 194–198 (2018).
14. Mahowald, N. M. et al. Aerosol deposition impacts on land and ocean carbon cycles. *Curr. Clim. Change Rep.* **3**, 16–31 (2017).
15. van der Werf, G. R. et al. Global fire emissions estimates during 1997–2016. *Earth Syst. Sci. Data* **9**, 697–720 (2017).
16. Evangeliou, N. et al. Open fires in Greenland in summer 2017: Transport, deposition and radiative effects of BC, OC, and BrC emissions. *Atmos. Chem. Phys.* **19**, 1393–1411 (2019).
17. Hamilton, D. S. et al. Earth, wind, fire, and pollution: Aerosol nutrient sources and impacts on ocean biogeochemistry. *Annu. Rev. Mar. Sci.* **14**, 303–330 (2022).
18. Soja, A. J., Shugart, H. H., Sukhinin, A., Conard, S. & Stackhouse, P. W. Satellite-derived mean fire return intervals as indicators of change in Siberia (1995–2002). *Mitig. Adapt. Strateg. Glob. Chang.* **11**, 75–96 (2006).
19. Ito, A. Mega fire emissions in Siberia: Potential supply of bioavailable iron from forests to the ocean. *Biogeosciences* **8**, 1679–1697 (2011).
20. Myriokefalitakis, S., Gröger, M., Hieronymus, J. & Döscher, R. An explicit estimate of the atmospheric nutrient impact on global oceanic productivity. *Ocean Sci.* **16**, 1183–1205 (2020).
21. Harrison, W. G. & Cota, G. F. Primary production in polar waters: Relation to nutrient availability. *Polar Res.* **10**, 87–104 (1991).
22. Tremblay, J.-É. et al. Global and regional drivers of nutrient supply, primary production and CO_2 drawdown in the changing Arctic Ocean. *Prog. Oceanogr.* **139**, 171–196 (2015).
23. Ardyna, M., Gosselin, M., Michel, C., Poulin, M. & Tremblay, J.-É. Environmental forcing of phytoplankton community structure and function in the Canadian High Arctic: contrasting oligotrophic and eutrophic regions. *Mar. Ecol. Prog. Ser.* **442**, 37–57 (2011).
24. Rainville, L. & Woodgate, R. A. Observations of internal wave generation in the seasonally ice-free Arctic. *Geophys. Res. Lett.* **36**, L23604 (2009).
25. Ardyna, M. et al. Recent Arctic Ocean sea-ice loss triggers novel fall phytoplankton blooms. *Geophys. Res. Lett.* **41**, 6207–6212 (2014).
26. Baumann, T. M. et al. On the seasonal cycles observed at the continental slope of the Eastern Eurasian Basin of the Arctic Ocean. *J. Phys. Oceanogr.* **48**, 1451–1470 (2018).
27. Bauch, D. & Cherniavskaia, E. Water mass classification on a highly variable Arctic shelf region: Origin of Laptev sea water masses and implications for the nutrient budget. *J. Geophys. Res. Oceans* **123**, 1896–1906 (2018).
28. Pnyushkov, A. V. et al. Heat, salt, and volume transports in the eastern Eurasian Basin of the Arctic Ocean from 2 years of mooring observations. *Ocean Sci.* **14**, 1349–1371 (2018).
29. Hölemann, J. A. et al. The impact of land-fast ice on the distribution of terrestrial dissolved organic matter in the Siberian Arctic shelf seas. *Biogeosci. Discuss* **2021**, 1–30 (2021).
30. Polyakov, I. V. et al. Greater role for Atlantic inflows on sea-ice loss in the Eurasian Basin of the Arctic Ocean. *Science* **356**, 285–291 (2017).
31. Lutsch, E. et al. Unprecedented atmospheric ammonia concentrations detected in the high Arctic from the 2017 Canadian wildfires. *J. Geophys. Res. Atmos.* **124**, 8178–8202 (2019).
32. Zhang, J., Li, D., Bian, J. & Bai, Z. Deep stratospheric intrusion and Russian wildfire induce enhanced tropospheric ozone pollution over the northern Tibetan Plateau. *Atmos. Res.* **259**, 105662 (2021).
33. Hurrell, J. W. et al. The Community Earth System Model: A framework for collaborative research. *Bull. Amer. Meteor. Soc.* **94**, 1339–1360 (2013).
34. Clark, S. K., Ward, D. S. & Mahowald, N. M. The sensitivity of global climate to the episodicity of fire aerosol emissions. *J. Geophys. Res.: Atmos.* **120**, 11,589–511,607 (2015).
35. Shi, J.-H. et al. Examination of causative link between a spring bloom and dry/wet deposition of Asian dust in the Yellow Sea, China. *J. Geophys. Res. Atmos.* https://doi.org/10.1029/2012JD017983 (2012).
36. Wiedinmyer, C. et al. The Fire INventory from NCAR (FINN): A high resolution global model to estimate the emissions from open burning. *Geosci. Model Dev.* **4**, 625–641 (2011).
37. Eckhardt, S. et al. Current model capabilities for simulating black carbon and sulfate concentrations in the Arctic atmosphere: a multi-model evaluation using a comprehensive measurement data set. *Atmos. Chem. Phys.* **15**, 9413–9433 (2015).
38. Hamilton, D. S. et al. Impact of changes to the atmospheric soluble iron deposition flux on ocean biogeochemical cycles in the anthropocene. *Glob. Biogeochem. Cycle* **34**, e2019GB006448 (2020).
39. Kramer, S. J., Bisson, K. M. & Fischer, A. D. Observations of phytoplankton community composition in the Santa Barbara channel during the Thomas fire. *J. Geophys. Res. Oceans* **125**, e2020JC016851 (2020).
40. Kim, Y., Hatsushika, H., Muskett, R. R. & Yamazaki, K. Possible effect of boreal wildfire soot on Arctic sea ice and Alaska glaciers. *Atmos. Environ.* **39**, 3513–3520 (2005).
41. Knapp, P. A. & Soulé, P. T. Spatio-temporal linkages between declining Arctic sea-ice extent and increasing wildfire activity in the Western United States. *Forests* **8**, 313 (2017).
42. Horvat, C. et al. The frequency and extent of sub-ice phytoplankton blooms in the Arctic Ocean. *Sci. Adv.* https://doi.org/10.1126/sciadv.1601191 (2017).
43. Ardyna, M. et al. Under-ice phytoplankton blooms: Shedding light on the "invisible" part of arctic primary production. *Front. Mar. Sci.* https://doi.org/10.3389/fmars.2020.608032 (2020).
44. Altieri, K. E., Fawcett, S. E. & Hastings, M. G. Reactive nitrogen cycling in the atmosphere and ocean. *Annu. Rev. Earth Planet. Sci.* https://doi.org/10.1146/annurev-earth-083120-052147 (2021).
45. Baker, A. R. & Jickells, T. D. Atmospheric deposition of soluble trace elements along the Atlantic Meridional Transect (AMT). *Prog. Oceanogr.* **158**, 41–51 (2017).
46. Hugelius, G. et al. Large stocks of peatland carbon and nitrogen are vulnerable to permafrost thaw. *Proc. Natl. Acad. Sci. USA* **117**, 20438–20446 (2020).
47. Schmale, J. et al. Pan-Arctic seasonal cycles and long-term trends of aerosol properties from 10 observatories. *Atmos. Chem. Phys.* **22**, 3067–3096 (2022).
48. Lewis, K. M., van Dijken, G. L. & Arrigo, K. R. Changes in phytoplankton concentration now drive increased Arctic Ocean primary production. *Science* **369**, 198–202 (2020).
49. Ardyna, M. & Arrigo, K. R. Phytoplankton dynamics in a changing Arctic Ocean. *Nat. Clim. Change* **10**, 892–903 (2020).
50. Tang, W. et al. Widespread phytoplankton blooms triggered by 2019–2020 Australian wildfires. *Nature* **597**, 370–375 (2021).
51. Fossheim, M. et al. Recent warming leads to a rapid borealization of fish communities in the Arctic. *Nat. Clim. Change* **5**, 673–677 (2015).
52. Sathyendranath, S. et al. An ocean-colour time series for use in climate studies: The experience of the Ocean-colour Climate Change Initiative (OC-CCI). *Sensors* **19**, 4285 (2019).
53. Gordon, H. R. & Wang, M. Retrieval of water-leaving radiance and aerosol optical thickness over the oceans with SeaWiFS: A preliminary algorithm. *Appl. Opt.* **33**, 443–452 (1994).
54. Werdell, P. J. & Bailey, S. W. An improved in-situ bio-optical data set for ocean color algorithm development and satellite data product validation. *Remote Sens. Environ.* **98**, 122–140 (2005).
55. Hu, C., Lee, Z. & Franz, B. Chlorophyll *a* algorithms for oligotrophic oceans: A novel approach based on three-band reflectance difference. *J. Geophys. Res. Oceans* https://doi.org/10.1029/2011JC007395 (2012).
56. Tilmes, S. et al. Description and evaluation of tropospheric chemistry and aerosols in the Community Earth System Model (CESM1.2). *Geosci. Model Dev.* **8**, 1395–1426 (2015).
57. Bernstein, D. et al. Short-term impacts of 2017 western North American wildfires on meteorology, the atmosphere's energy budget, and premature mortality. *Environ. Res. Lett.* **16**, 064065 (2021).
58. Liu, X. et al. Description and evaluation of a new four-mode version of the Modal Aerosol Module (MAM4) within version 5.3 of the Community Atmosphere Model. *Geosci. Model Dev.* **9**, 505–522 (2016).
59. Suarez, M. J. et al. The GEOS-5 Data Assimilation System – Documentation of Versions 5.0.1, 5.1.0, and 5.2.0. No. NASA/TM-2008-104606-VOL-27 (2008).
60. Janssens-Maenhout, G. et al. HTAP_v2.2: A mosaic of regional and global emission grid maps for 2008 and 2010 to study hemispheric transport of air pollution. *Atmos. Chem. Phys.* **15**, 11411–11432 (2015).

61. Dentener, F. et al. Emissions of primary aerosol and precursor gases in the years 2000 and 1750 prescribed data-sets for AeroCom. *Atmos. Chem. Phys.* **6**, 4321–4344 (2006).
62. Inness, A. et al. The CAMS reanalysis of atmospheric composition. *Atmos. Chem. Phys.* **19**, 3515–3556 (2019).
63. Stein, A. F. et al. NOAA's HYSPLIT atmospheric transport and dispersion modeling system. *Bull. Am. Meteorol. Soc.* **96**, 2059–2077 (2015).
64. Carter, T. S. et al. How emissions uncertainty influences the distribution and radiative impacts of smoke from fires in North America. *Atmos. Chem. Phys.* **20**, 2073–2097 (2020).
65. Pan, X. et al. Six global biomass burning emission datasets: Intercomparison and application in one global aerosol model. *Atmos. Chem. Phys.* **20**, 969–994 (2020).
66. Reddington, C. L. et al. Analysis of particulate emissions from tropical biomass burning using a global aerosol model and long-term surface observations. *Atmos. Chem. Phys.* **16**, 11083–11106 (2016).
67. Kiely, L. et al. New estimate of particulate emissions from Indonesian peat fires in 2015. *Atmos. Chem. Phys.* **19**, 11105–11121 (2019).
68. Giglio, L., Boschetti, L., Roy, D. P., Humber, M. L. & Justice, C. O. The Collection 6 MODIS burned area mapping algorithm and product. *Remote Sens. Environ.* **217**, 72–85 (2018).
69. Arrigo, K. R. et al. Phytoplankton blooms beneath the sea ice in the Chukchi Sea. *Deep Sea Res. Pt. 2* **105**, 1–16 (2014).
70. Geider, R. J., Maclntyre, H. L. & Kana, T. M. A dynamic regulatory model of phytoplanktonic acclimation to light, nutrients, and temperature. *Limnol. Oceanogr.* **43**, 679–694 (1998).
71. Liefer, J. D., Garg, A., Campbell, D. A., Irwin, A. J. & Finkel, Z. V. Nitrogen starvation induces distinct photosynthetic responses and recovery dynamics in diatoms and prasinophytes. *PLoS One* **13**, e0195705 (2018).

Acknowledgements

M.A. was supported by the Alg-O-Nord research project of the CNES (Center National d'Etudes Spatiales), High Impact Publications Program of ArcticNet and a European Union's Horizon 2020 Marie Sklodowska-Curie grant (no. 746748). This work represents a contribution to IRL Takuvik, Stanford University, Sorbonne Université, Sentinelle Nord, Québec Océan and Institut Nordique du Québec. We would like to thank the international agencies and programs for support, including the U.S. Department of Energy (DOE, grant Number: DE-SC0021302) and Cornell Atkinson Center for Sustainability. We would like to acknowledge the computational resources from Cheyenne provided by NCAR's Computational and Information Systems Laboratory, sponsored by the National Science Foundation. The authors gratefully acknowledge the NOAA Air Resources Laboratory (ARL) for the provision of the HYSPLIT transport and dispersion model used in this publication. Geostrophic currents data were provided by the Center for Polar Observation and Modeling, University College London (www.cpom.ucl.ac.uk/dynamic_topography). Sea ice extent was computed based on the sea ice concentration product (SIC) provided by the ERA5 (https://www.ecmwf.int). Bathymetry data was freely provided by GEBCO Compilation Group (2020) GEBCO 2020 Grid (https://doi.org/10.5285/a29c5465-b138-234d-e053-6c86abc040b9). We finally thank Marcel Babin for his comments and useful suggestions for improving the manuscript.

Author contributions

M.A., D.S.H., T.H., L.L., D.N.B., J.L., C.H., R.L., M.M.M., G.v.D., and I.P. conducted the data analysis. M.A, D.S.H., D.N.B., and C.H. wrote the manuscript. D.N.B. ran the Community Earth System Model simulations. M.A., D.S.H., T.H., L.L., D.N.B., J.L., C.H., R.L., M.M.M., G.v.D., I.P., H.C., N.M., and K.R.A. contributed to the ideas and commented on the manuscript.

Competing interests

The authors declare no competing interests.

Additional information

Supplementary information The online version contains supplementary material available at https://doi.org/10.1038/s43247-022-00511-9.

Correspondence and requests for materials should be addressed to Mathieu Ardyna.

Peer review information *Communications Earth & Environment* thanks Tymon Zielinski and the other anonymous reviewer(s) for their contribution to the peer review of this work. Primary Handling Editors: Clare Davis. Peer reviewer reports are available.

Reprints and permission information is available at http://www.nature.com/reprints

Publisher's note Springer Nature remains neutral with regard to jurisdictional claims in published maps and institutional affiliations.

Open Access This article is licensed under a Creative Commons Attribution 4.0 International License, which permits use, sharing, adaptation, distribution and reproduction in any medium or format, as long as you give appropriate credit to the original author(s) and the source, provide a link to the Creative Commons license, and indicate if changes were made. The images or other third party material in this article are included in the article's Creative Commons license, unless indicated otherwise in a credit line to the material. If material is not included in the article's Creative Commons license and your intended use is not permitted by statutory regulation or exceeds the permitted use, you will need to obtain permission directly from the copyright holder. To view a copy of this license, visit http://creativecommons.org/licenses/by/4.0/.

© The Author(s) 2022